EurJIC
European Journal of Inorganic Chemistry

Full Papers
doi.org/10.1002/ejic.202000954

Chemistry Europe
European Chemical Societies Publishing

Magnetic Molecular Rectangles Constructed from Functionalized Nitronyl-Nitroxide Ligands and Lanthanide(III) Ions

Sergiu Calancea,[a, b] Luca Carrella,[c] Teodora Mocanu,[a, e] Vladimir Sadohin,[b] Mihai Raduca,[a] Iacob Gutu,[b] Julio C. da Rocha,[d] Maria G. F. Vaz,[d] Eva Rentschler,*[c] and Marius Andruh*[a]

Dedicated to Professor Alexandru T. Balaban on the occasion of his 90th birthday.

Five binuclear complexes with rectangular topology have been synthesized using a nitronyl-nitroxide ligand (L) functionalized with a pyrazole coordinating group: $[Ln_2(hfac)_2L_2]$, with Ln = Eu (**1**), Gd (**2a**, **2b**), Tb (**3**), Dy (**4**), Tm (**5**). The Eu^{III} and Tm^{III} complexes crystallize in the $P2_1/n$ space group, while the Gd^{III}, Tb^{III}, and Dy^{III} derivatives crystalize in *P*-1 space group. The crystal structures for compounds **2a**, **3**, **4**, and **5** have been fully solved, while for compounds **1** and **2b**, the unit cell parameters have been measured and compared with crystals **3** and **5**. Crystals **2a** ($P2_1/n$) and **2b** (*P*-1) are polymorphic forms. In these complexes the nitronyl-nitroxide ligand bridges two metal ions through one aminoxyl group and the pyrazole fragment. In the five complexes the Ln^{III} ions show a coordination number of eight with a triangular dodecahedron geometry. The magnetic properties of all five complexes have been investigated. For compounds **2**, **3**, and **4** the Ln^{III}-Rad interaction was found to be ferromagnetic: $J_{GdRad} = 2.09(1)\ cm^{-1}$ [$\boldsymbol{H} = -2J_{GdRad}(\boldsymbol{S}_{Gd1}\boldsymbol{S}_{Rad1} + \boldsymbol{S}_{Gd2}\boldsymbol{S}_{Rad2}]$, $J_{TbRad} = 1.93(14)\ cm^{-1}$, $J_{DyRad} = 1.72(14)\ cm^{-1}$. The Tm^{III}-Rad coupling is antiferromagnetic ($J_{TmRad} = -0.53(1)\ cm^{-1}$). For the Tb^{III}, Dy^{III}, and Tm^{III} complexes the effects of the crystal field have been taken into account in the fitting procedure.

Introduction

Metal-nitronyl-nitroxide complexes represent a large class of molecular magnetic materials.[1] The paramagnetic nitronyl-nitroxide species can act as ligands towards *d* and *f* transition metal ions, and generate either discrete species or coordination polymers.[1] The very first Single Chain Magnet that opened a new era in molecular magnetism is a cobalt(II) 1D coordination polymer constructed from a nitronyl-nitroxide ligand, 4′-methoxy-phenyl-4,4,5,5-tetramethylimidazoline-1-oxyl-3-oxide, that bridges the metal ions.[2] The richness of this chemistry is due to the availability of a practically unlimited number of aldehydes which can be synthesized and transformed into nitronyl-nitroxide radicals (Nit) following or adapting Ullman's synthetic approach.[3] As such, the nitronyl-nitroxide radical can be decorated with various coordinating groups, R, neutral or anionic, which play a key role on the dimensionality and spin topologies of the resulting complexes.[1,5] The structural diversity of metal-NitR systems arises from several factors: (i) the different coordination modes of the nitronyl-nitroxid moiety (terminal, bridging through both aminoxyl groups, bridging through only one aminoxyl group); (ii) the number and the relative positions of the donor atoms of the organic groups (R) attached to the Nit fragment; (iii) the number of the Nit fragments within the paramagnetic organic ligands; (iv) the nature of the anions accompanying the metal ions (frequently fluorinated β-diketonates, carboxylates, halocarboxylates); (v) the stereochemical preference of the metal ion. Generally, the resulting structures of these heterospin systems cannot be easily predicted. However, the obtained complexes show interesting magnetic properties and serve as models for magneto-structural correla-

[a] *Dr. S. Calancea, T. Mocanu, M. Raduca, Prof. M. Andruh*
Inorganic Chemistry Laboratory,
Faculty of Chemistry,
University of Bucharest,
Str. Dumbrava Rosie nr. 23, 020464, Bucharest, Romania
E-mail: marius.andruh@dnt.ro
[b] *Dr. S. Calancea, V. Sadohin, Prof. I. Gutu*
Moldova State University,
Faculty of Chemistry and Chemical, Technology,Chişinău,
2009-Chisinau, Moldova
[c] *Dr. L. Carrella, Prof. E. Rentschler*
Department of Chemistry,
Johannes Gutenberg University Mainz
Duesbergweg 10–14, 55128- Mainz, Germany
E-mail: rentschl@uni-mainz.de
[d] *Dr. J. C. da Rocha, Prof. M. G. F. Vaz*
Universidade Federal Fluminense,
Instituto de Química,
24020-346-Niterói, Rio de Janeiro, Brazil
[e] *T. Mocanu*
Coordination and Supramolecular Chemistry Laboratory,
"Ilie Murgulescu"
Institute of Physical Chemistry,
Romanian Academy,
Splaiul Independentei 202,
Bucharest 060021, Romania

Supporting information for this article is available on the WWW under https://doi.org/10.1002/ejic.202000954

tions. More recently, this chemistry has been enriched with a new class, namely heterotrispin 2*p*-3*d*-4*f* complexes.[6] We have shown that, using compartmental ligands bearing a NitR arm, strictly binuclear 3*d*-4*f* complexes can be rationally designed.[7]

The magnetic interaction between the two spin carriers 2*p*-n*d* or 2*p*-4*f* vary between strong antiferro- and strong ferromagnetic couplings.[1] The nature and strength of the exchange interaction depends on several factors, emphasized by a plethora of magneto-structural studies. In a nutshell: the 2*p*-n*d* interactions are stronger than the 2*p*-4*f* ones and the geometric parameters, at the level of aminoxyl-metal bond, influence the orientation of the magnetic orbitals π^* (Nit) and *d* or *f* and thus their overlap or orthogonality. It is important to note that the paramagnetic lanthanide(III) and europium(III) ions which are characterized by an important magnetic anisotropy, except gadolinium(III), are good candidates for the observation of the slow relaxation of the magnetization phenomena. We recall that the ground state of europium(III) is $J=0$ and, consequently, its complexes are diamagnetic at low temperatures.

Regarding the structural types of binuclear Ln^{III}-NitR complexes, the two lanthanide ions can be held together: (a) by NitR ligands that simultaneously chelate and bridge the metal ions (Scheme 1A, where X is phenoxido oxygen atom);[8] (b) by NitR spacers coordinated with the Nit end to one lanthanide and with the other end, R, to the second lanthanide ion (Scheme 1B, where Y is generally a nitrogen atom);[9] (c) by NitR ligands acting in bis-chelating bridging mode (Scheme 1C, where Z are nitrogen atoms arising from a pyrimidine fragment).[10] In this paper, we report on new $[Ln_2(NitR)_2]$ complexes, which belong to the second structural type (Scheme 1B).

Results and Discussion

Description of the structures

Five binuclear isostructural complexes have been assembled using the new ligand L, which is synthesized as illustrated in Scheme 2. In principle, the pyrazole intermediate, obtained in the second step, can be decorated with various groups, pre-attached to the phenyl ring of the starting acetophenone. These ancillary groups can coordinate to the metal ions or/and influence the solubility of the resulting complexes as well as their packing in the crystal. The pyrazole ring is expected to coordinate to a metal ion through the 2-N atom (sp^2).[11] The new complexes have the general formula $[Ln_2(hfac)_2L_2]$, with Ln = Eu (**1**), Gd (**2a**,**2b**), Tb (**3**), Dy (**4**), Tm (**5**), and have been synthesized by reacting L with $Ln(hfac)_3 \cdot 3H_2O$. The single crystal X-ray diffraction studies reveal that these compounds have similar structures belonging to the prototype **B** depicted in Scheme 1. Compounds **1**, **2a** and **5** crystallize in the monoclinic $P2_1/n$ space group, while compounds **2b**, **3** and **4** crystallize in the triclinic *P*-1 space group. We succeeded to solve and fully refine the crystal structures for compounds **2a**, and **3–5** (Table 1). The measurements of the unit cell parameters for crystals **1**, **2b** and **4** show that **1**, **2a** and **5** and, respectively, **2b**, **3** and **4** are isomorphous (Table S1). The powder X-Ray diffraction patterns for compounds **1–4** are presented in

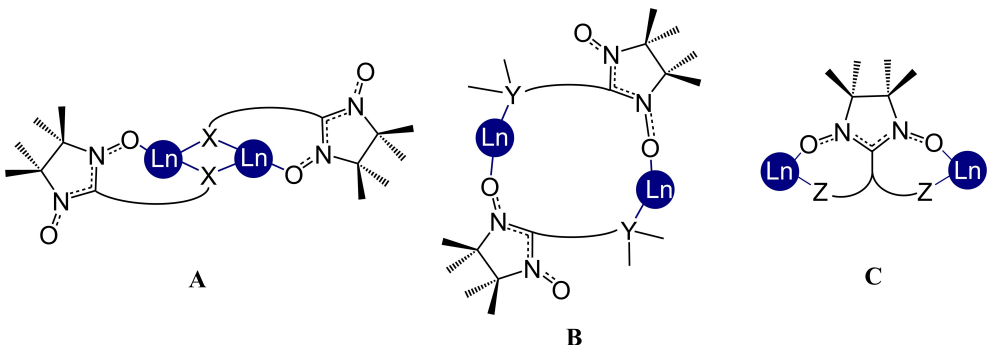

Scheme 1. Different coordination modes of nitronyl nitroxides in binuclear Ln^{III}-NitR complexes.

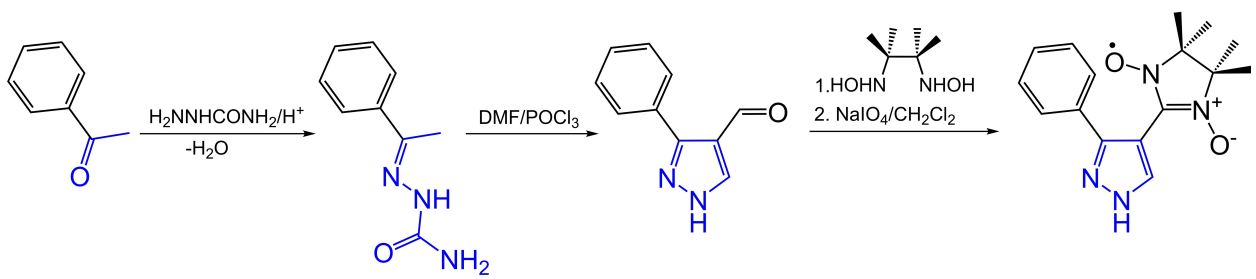

Scheme 2. Reaction scheme for the synthesis of 3-phenyl-1H-pyrazole-4-nitronyl nitroxide

Table 1. Crystal data and structure refinement parameters for complexes **2a**, **3**, **4**, and **5**.

	2a	3	4	5
Formula sum	$C_{31}H_{22}GdF_{18}N_4O_8$	$C_{31}H_{22}TbF_{18}N_4O_8$	$C_{31}H_{22}DyF_{18}N_4O_8$	$C_{31}H_{22}TmF_{18}N_4O_8$
Formula weight	1077.77	1079.44	1083.02	1088.45
Crystal system	monoclinic	triclinic	triclinic	monoclinic
Space group	$P2_1/n$	P-1	P-1	$P2_1/n$
a/Å	14.1094(14)	12.0151(16)	11.9820(6)	14.1344(7)
b/Å	19.3952(18)	12.777(3)	12.7361(7)	19.2831(8)
c/Å	15.0889(14)	15.161(3)	15.1509(8)	15.0771(7)
α/°	90.000	70.025(14)	70.100(2)	90.000
β/°	105.521(3)	69.273(11)	69.370(2)	104.581(4)
γ/°	90.000	87.271(14)	87.416(2)	90.000
V/Å^3	3978.6(7)	2038.6(7)	2027.2(2)	3977.0(3)
Z	4	2	2	4
D_c/g cm^{-3}	1.799	1.758	1.774	1.818
T/K	293.15	293(2)	293.15	293.15
μ/mm^{-1}	1.803	1.867	1.977	2.367
Reflections collected	118722	21353	85523	44637
Independent reflection	6993 [R_{int} = 0.1898]	7170 [R_{int} = 0.0848]	9706 [R_{int} = 0.0433]	6997 [R_{int} = 0.1834]
R_1[a] [$I > 2\sigma(I)$]	0.0628	0.0578	0.0345	0.0653
wR_2[b] (all data)	0.1569	0.1313	0.0953	0.1430
GOF	1.084	1.005	1.154	1.080
$\Delta\rho_{min}/\Delta\rho_{max}$ (e Å^{-3})	−0.88/1.19	−0.55/0.81	−0.97/2.55	−0.91/1.00

[a] $R_1 = \Sigma||F_o|-|F_c||/\Sigma|F_o|$. [b] $wR_2 = [\Sigma w(F_o^2-F_c^2)^2/\Sigma w(F_o^2)^2]^{1/2}$; $w = 1/[\sigma^2(F_0^2)+(aP)^2+bP]$ where $P = [\max(F_0^2, 0)+2F_c^2]/3$.

Figures S1.1–S1.4 and show that **1**, **3**, and **4** are pure crystalline phases, while the crystalline powder of **2** contains **2a** ($P2_1/n$, minor component) and **2b** (P-1, major component). Crystals **2a** and **2b** are polymorphic forms and differ only by the packing of the same binuclear molecules in the crystals (see below). We will describe here only the crystal structure of **3** (Figure 1). The asymmetric unit contains one lanthanide ion, three $hfac^-$ ions and one paramagnetic ligand molecule. The nitronyl-nitroxide ligand bridges two metal ions through one aminoxyl group and the pyrazole fragment. The Tb^{III} ions are eight-coordinated by six oxygen atoms from the chelating hfac anions (Tb1−O3 = 2.384(5), Tb1−O4 = 2.317(6), Tb1−O5 = 2.414(5), Tb1−O6 = 2.347(6), Tb1−O7 = 2.333(6), Tb1−O8 = 2.390(6) Å), one nitroxide oxygen atoms arising from one L molecules and one pyrazole nitrogen from the second radical molecule (Tb1−O2 = 2.296(5), Tb1−N4^a = 2.575(6) Å, $^a = 1-x, 1-y, -z$). The coordination geometry of the metal centers was assigned as triangular dodecahedron, according to the shape measure parameters calculated using SHAPE program[12] (Tabel S2). The same stereochemistry was found for Ln^{III} ions in **2a**, **4**, and **5**. The two metal centers of the binuclear complex adopt opposite chiral configurations (lambda and delta) (Figure 1). The intramolecular Tb···Tb distance is 7.007 Å. The dissimilarities between the compounds that crystalize in the triclinic and monoclinic systems arise from the packing of the binuclear complexes. In the case of crystal **3** (Figure 2) the binuclear units associate in supramolecular chains built through CH···O contacts established between the CH_3 groups and uncoordinated NO arms (C6···O1^b = 3.584 Å, H6 C···O1^b = 2.628 Å, C6−H6 C···O1^b = 173.9°; C3···O1^b = 3.358 Å, H3 A···O1^b = 2.588 Å, C3−H3 A···O1^b = 137.4°; $^b = -x, 1-y, -z$). On the other hand, for compound **5** (Figure 3) a 2-D halogen-bonded network is built from the binuclear entities through F···F interactions (F9B···F18B^a = 2.891 Å, F17B···F10^b = 2.883 Å, F18 A···F10^b = 2.791 Å, F16 A···F5^c = 2.933 Å, $^a = -0.5-x, 0.5+y, 0.5-z$, $^b = 0.5+x, -0.5-y, 0.5+z$, $^c = -0.5+x, -0.5-y, 0.5+z$). For each of the two models found for the disordered CF_3 groups, the distances of F···F interactions are shorter than the sum of van der Waals radii of two fluorine atoms (2.94 Å).[13] Selected bond distances and angles for compounds **3** and **5** are collected in Table 2.

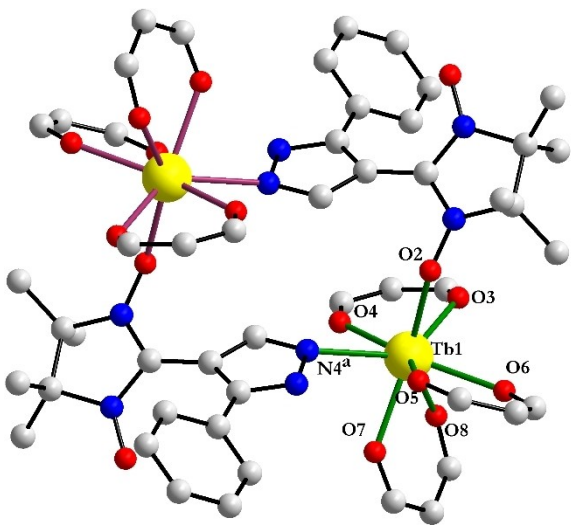

Figure 1. Perspective view of $[Tb_2(hfac)_2L_2]$ **3** showing the opposite chiral configurations (lambda - violet and delta - green) of Tb^{III} ions and atom numbering scheme (symmetry code: $^a = 1-x, 1-y, -z$). The CF_3 groups have been omitted, for clarity.

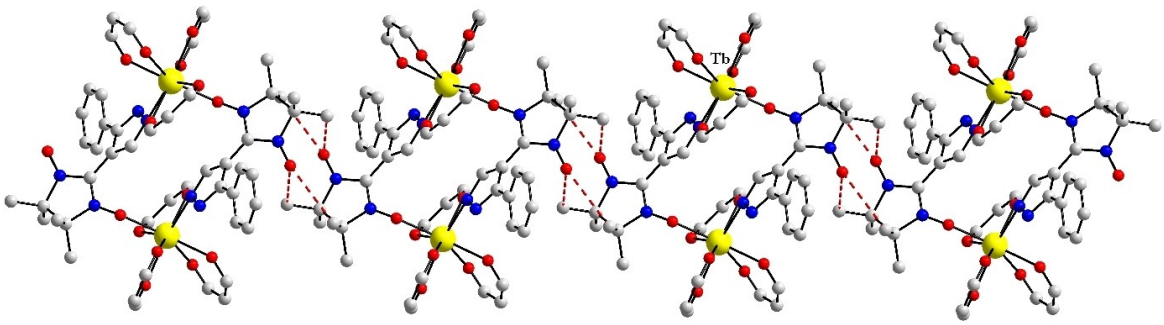

Figure 2. Packing diagram for crystal **3**, showing the supramolecular chains resulted from CH···O interactions. The CF_3 groups from the hfac ligands have been omitted for clarity.

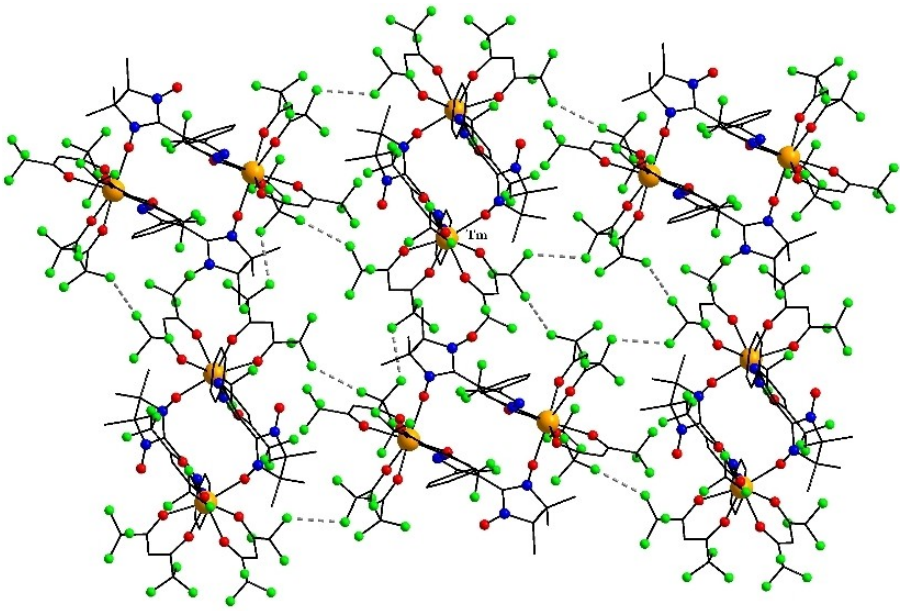

Figure 3. Packing diagram for crystal **5**, showing the supramolecular layers.

Magnetic properties

The cryomagnetic behavior of compounds **1–5** has been investigated. We discuss first the magnetic properties of the gadolinium derivative, **2** (Figure 4). The magnetic measurements were carried out on the mixture of **2a** and **2b**, the magnetic properties of the two polymorphs are treated together, since the molecular structures of **2a** and **2b** are similar. The different packings of the molecules in the crystals will only influence the weak, if any, intermolecular interactions. The room temperature value of the $\chi_M T$ product is 16.53 $cm^3 Kmol^{-1}$, that corresponds perfectly to four uncoupled spins with $S_1 = S_2 = {}^1/_2$ and $S_3 = S_4 = {}^7/_2$. By lowering the temperature to 16 K a smooth increase is observed, while further cooling leads to a drop of $\chi_M T$ to 11.57 $cm^3 Kmol^{-1}$. The increase of the $\chi_M T$ product indicates a ferromagnetic interaction between the Gd^{III} ions and the radicals, while the sharp drop results from weak antiferromagnetic interactions. At low temperatures, the magnetization saturates at high fields to a value of 16.08 $N\mu_B$, in perfect agreement with the expected value of 16.00 $N\mu_B$ (inset to Figure 4). Both, susceptibility and magnetization data, have been fitted simultaneously ($g = 2.00$, fixed value) resulting in $J_{GdRad} = 2.09(1)$ cm^{-1} [$\boldsymbol{H} = -2J_{GdRad}(\boldsymbol{S}_{Gd1}\boldsymbol{S}_{Rad1} + \boldsymbol{S}_{Gd2}\boldsymbol{S}_{Rad2})$]. Only the interactions between the radicals and gadolinium ions have been taken into account. The drop of $\chi_M T$ at low temperatures has been modelled with a weak antiferromagnetic mean field interaction, zJ=-0.0187(1) cm^{-1}, which can arise from Gd^{III}-Gd^{III} coupling, and/or intermolecular interactions. The ferromagnetic interaction between Gd^{III} and the aminoxyl group is generally weak (few wavenumbers) and, according to magneto-structural correlations supported by theoretical calculations, it is influenced by the Gd-N–O angles and Gd-O–N-C dihedral angles.[15] Large Gd-O–N-C angles favor the ferromagnetic couplings. The values of these angles for the terbium derivative (Tb–N–O = 140.43 and Tb–O–N–C = 84.10°) support the sign and value obtained for J_{GdRad}, by comparing with other Gd^{III}-Rad complexes collected in ref.[15]

Table 2. Selected bond distance and angles for compounds **2a**, **3**, **4**, and **5**.

2a		3		4		5	
Gd1–O2[a]	2.312(7)	Tb1–O2	2.296(5)	Dy1–O2	2.294(2)	Tm1–O2[c]	2.258(7)
Gd1–O3	2.385(6)	Tb1–O3	2.384(5)	Dy1–O3	2.371(3)	Tm1–O3	2.308(7)
Gd1–O4	2.371(6)	Tb1–O4	2.317(6)	Dy1–O4	2.313(3)	Tm1–O4	2.331(7)
Gd1–O5	2.356(7)	Tb1–O5	2.414(4)	Dy1–O5	2.396(3)	Tm1–O5	2.308(9)
Gd1–O6	2.370(7)	Tb1–O6	2.347(6)	Dy1–O6	2.333(3)	Tm1–O6	2.357(8)
Gd1–O7	2.356(6)	Tb1–O7	2.333(6)	Dy1–O7	2.328(3)	Tm1–O7	2.303(8)
Gd1–O8	2.410(6)	Tb1–O8	2.390(6)	Dy1–O8	2.380(3)	Tm1–O8	2.348(7)
Gd1–N4	2.543(7)	Tb1–N4[b]	2.575(6)	Dy1–N4[b]	2.562(3)	Tm1–N4	2.501(9)
O2[a] Gd1 O3	87.8(2)	O2 Tb1 O3	75.6(2)	O2 Dy1 O3	75.6(1)	O2[c] Tm1 O3	87.4(3)
O2[a] Gd1 O4	77.7(2)	O2 Tb1 O4	100.1(2)	O2 Dy1 O4	100.2(1)	O2[c] Tm1 O4	93.8(3)
O2[a] Gd1 O5	148.8(2)	O2 Tb1 O5	73.1(2)	O2 Dy1 O5	73.1(1)	O2[c] Tm1 O5	148.6(3)
O2[a] Gd1 O6	141.1(2)	O2 Tb1 O6	90.4(2)	O2 Dy1 O6	90.5(1)	O2[c] Tm1 O6	140.0(3)
O2[a] Gd1 O7	90.0(2)	O2 Tb1 O7	143.0(2)	O2 Dy1 O7	142.9(1)	O2[c] Tm1 O7	91.9(3)
O2[a] Gd1 O8	73.0(2)	O2 Tb1 O8	143.5(2)	O2 Dy1 O8	143.1(2)	O2[c] Tm1 O8	71.5(3)
O2[a] Gd1 N4	94.6(2)	O2 Tb1 N4[b]	86.4(2)	O2 Dy1 N4[b]	86.1(1)	O2[c] Tm1 N4	93.8(3)
O3 Gd1 O4	72.0(2)	O3 Tb1 O4	71.9(2)	O3 Dy1 O4	72.3(1)	O3 Tm1 O4	73.9(3)
O3 Gd1 O5	74.4(2)	O3 Tb1 O5	138.0(2)	O3 Dy1 O5	137.8(2)	O3 Tm1 O5	74.5(3)
O3 Gd1 O6	122.1(2)	O3 Tb1 O6	82.0(2)	O3 Dy1 O6	81.2(2)	O3 Tm1 O6	122.3(3)
O3 Gd1 O7	148.5(2)	O3 Tb1 O7	140.5(2)	O3 Dy1 O7	140.4(2)	O3 Tm1 O7	147.9(3)
O3 Gd1 O8	135.8(2)	O3 Tb1 O8	70.3(2)	O3 Dy1 O8	69.8(2)	O3 Tm1 O8	135.0(3)
O3 Gd1 N4	71.0(2)	O3 Tb1 N4[b]	134.0(2)	O3 Dy1 N4[b]	134.5(1)	O3 Tm1 N4	70.9(3)
O4 Gd1 O5	72.5(3)	O4 Tb1 O5	140.6(2)	O4 Dy1 O5	140.6(1)	O4 Tm1 O5	72.4(3)
O4 Gd1 O6	131.9(2)	O4 Tb1 O6	148.2(2)	O4 Dy1 O6	147.7(2)	O4 Tm1 O6	132.1(3)
O4 Gd1 O7	76.9(2)	O4 Tb1 O7	100.2(2)	O4 Dy1 O7	100.1(2)	O4 Tm1 O7	141.1(3)
O4 Gd1 O8	137.1(2)	O4 Tb1 O8	81.8(2)	O4 Dy1 O8	81.5(2)	O4 Tm1 O8	135.0(3)
O4 Gd1 N4	142.4(2)	O4 Tb1 N4[b]	70.1(2)	O4 Dy1 N4[b]	70.4(2)	O4 Tm1 N4	144.2(3)
O5 Gd1 O6	69.3(2)	O5 Tb1 O6	71.0(2)	O5 Dy1 O6	71.6(1)	O5 Tm1 O6	70.6(3)
O5 Gd1 O7	92.3(3)	O5 Tb1 O7	71.5(2)	O5 Dy1 O7	71.4(2)	O5 Tm1 O7	90.4(3)
O5 Gd1 O8	137.0(2)	O5 Tb1 O8	126.9(2)	O5 Dy1 O8	127.2(1)	O5 Tm1 O8	138.7(3)
O5 Gd1 N4	103.1(3)	O5 Tb1 N4[b]	70.8(2)	O5 Dy1N4[b]	70.3(2)	O5 Tm1 N4	103.8(3)
O6 Gd1 O7	76.7(3)	O6 Tb1 O7	88.3(2)	O6 Dy1 O7	88.4(2)	O6 Tm1 O7	76.4(3)
O6 Gd1 O8	68.2(2)	O6 Tb1 O8	72.4(2)	O6 Dy1 O8	72.0(2)	O6 Tm1 O8	68.6(3)
O6 Gd1 N4	75.3(3)	O6 Tb1 N4[b]	140.9(2)	O6 Dy1 N4[b]	141.1(1)	O6 Tm1 N4	74.7(3)
O7 Gd1 O8	72.5(2)	O7 Tb1 O8	70.3(2)	O7 Dy1 O8	70.6(1)	O7 Tm1 O8	74.1(3)
O7 Gd1 N4	140.5(2)	O7 Tb1 N4[b]	72.0(2)	O7 Dy1 N4[b]	72.0(2)	O7 Tm1 N4	141.1(3)
O8 Gd1 N4	71.5(2)	O8 Tb1 N4[b]	127.2(2)	O8 Dy N4[b]	127.7(2)	O8 Tm1 N4	71.4(2)

[a] = 1−x, 1−y, 1−z. [b] = 1−x, 1−y, −z. [c] = −x, −y, 1−z.

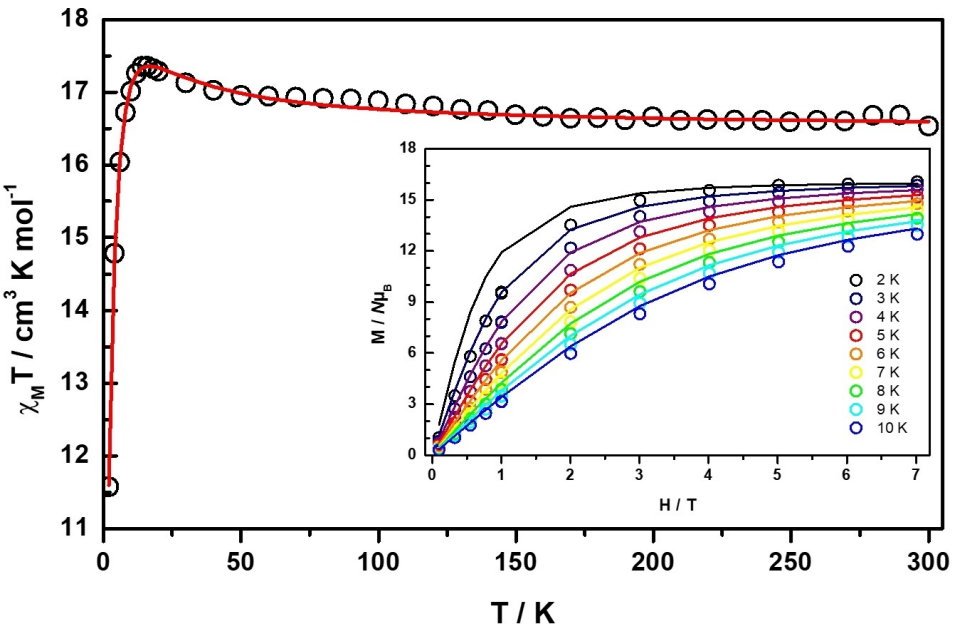

Figure 4. Temperature dependence of the $\chi_M T$ product for compound **2**. Inset: field dependence of the magnetization at various temperatures. The solid lines correspond to the best fit with the parameters indicated in the text.

The room temperature $\chi_M T$ value for compound **3**, 25.19 $cm^3 mol^{-1} K$, is slightly higher than the calculated one (24.41 $cm^3 Kmol^{-1}$) for two non-interacting radicals ($S_1 = S_2 = {}^1/_2$) and two Tb^{III} ions ($^7F_6$, $S = 3$, $L = 3$, $g = 3/2$). The values of the $\chi_M T$ product remain nearly constant upon cooling down to 30 K. Below this temperature, a significant decrease is observed, reaching 9.55 $cm^3 Kmol^{-1}$ at 2 K (Figure 5). The field dependence of the magnetization shows a saturation-like behaviour at high fields. However, the magnetization value at 2 K and 7 Tesla (11.83 $N_i\mu_B$) lies significantly below the expected value (20 $N_i\mu_B$), indicating strong crystal field effects (CF; $\boldsymbol{H}_{CF} = \sum_{k=2,4,6} \sum_{q=0}^{k} B_k^q O_k^q$).[14] In order to estimate the contribution and the sign of the CF, the magnetic data were simulated first without any CF and then with CF (B_2^0, positive and negative; other terms are not included in order to avoid overparameterization), the other parameters being fixed to the values obtained for compound **2**. Thereafter, all parameters (J, zJ, CF) were freely refined. Good fits of the temperature dependent susceptibility are obtained by including a CF parameter (B_2^0), both positive and negative (Figure S2). However, for the field dependent data, a good simulation is obtained only with a negative CF parameter (Figures S3 and S4). Once the sign of the CF parameter was determined, all the others were freely refined. An improvement in the quality of the simulation was obtained with the following values: $g_{Rad} = 2.00$, $g_{Tb} = 1.5$, $J_{TbRad} = 2.97(22)\,cm^{-1}$, $zJ = -0.0199(1)\,cm^{-1}$, $B_2^0 = -2.25(20)\,cm^{-1}$ (Figure S5). However, in particular in the high temperature range of the temperature dependence of $\chi_M T$, a significant deviation between simulation and data is observed. To further improve the fitting, the g value of Tb^{III} ions was increased to 1.53. This leads to a significant improvement with the following parameters: $g_{Rad} = 2.000$, $g_{Tb} = 1.53$, $J_{TbRad} = 1.93(14)\,cm^{-1}$, $zJ = -0.0208(4)\,cm^{-1}$, $B_2^0 = -3.84(36)\,cm^{-1}$ (Figure 5). A good fit of the magnetization versus field data is obtained with the same parameters (inset to Figure 5). The presence of magnetic anisotropy may lead to the observation of single molecular behavior. However, no out of phase signal can be detected in the ac measurements for **3**.

The magnetic data for the dysprosium derivative, **4**, are displayed in Figure 6. The room temperature value of the $\chi_M T$ product (29.68 $cm^3 Kmol^{-1}$) corresponds well to the one calculated (29.08 $cm^3 Kmol^{-1}$) for two non-interacting radicals ($S_1 = S_2 = {}^1/_2$) and two dysprosium(III) ions ($^6H_{15/2}$, $S = 5/2$, $L = 5$, $g = 4/3$). The value remains nearly constant upon cooling. Only at temperatures below 16 K a significant decrease can be observed, reaching 8.45 $cm^3 Kmol^{-1}$ at 2 K. The field dependence of the magnetization shows a rapid increase at low fields without reaching saturation at 7 Tesla, indicating magnetic anisotropy. Furthermore, the magnetization value at 2 K and 7 Tesla of 13.39 $N\mu_B$, which is much lower than the calculated one of 22 $N\mu_B$, is characteristic for strong crystal field effects (CF). The magnetic data have been treated following the same procedure as for compound **3**. In order to estimate the contribution and the sign of CF, the magnetic data were simulated first without any CF and then with CF (positive and negative), while fixing all the other parameters to the values obtained from compound **2** (Figures S6–S8). A good fit of the temperature dependence of the $_{\chi M}T$ product can be obtained taking a small CF (B_2^0) of $+2.38(21)\,cm^{-1}$ or $-2.94(98)\,cm^{-1}$ into account. Without any CF, the deviation is much larger. To estimate the sign of the CF the field dependence of the magnetisation has to be taken into account. No good fit of the magnetization data can be obtained, either with positive CF or without CF, while a good fit can be obtained with a negative CF parameter. The best fit parameters are: $g_{Rad} = 2.00$; $g_{Dy} = 1.333$, $J_{DyRad} = 1.72(14)\,cm^{-1}$, $zJ = -0.0248(5)\,cm^{-1}$, $B_2^0 = -1.47(22)\,cm^{-1}$. However, small deviations between simulation and experimental data can be observed. These may result from higher CF-terms (e.g. B_2^2) or deviation from the ideal coordination

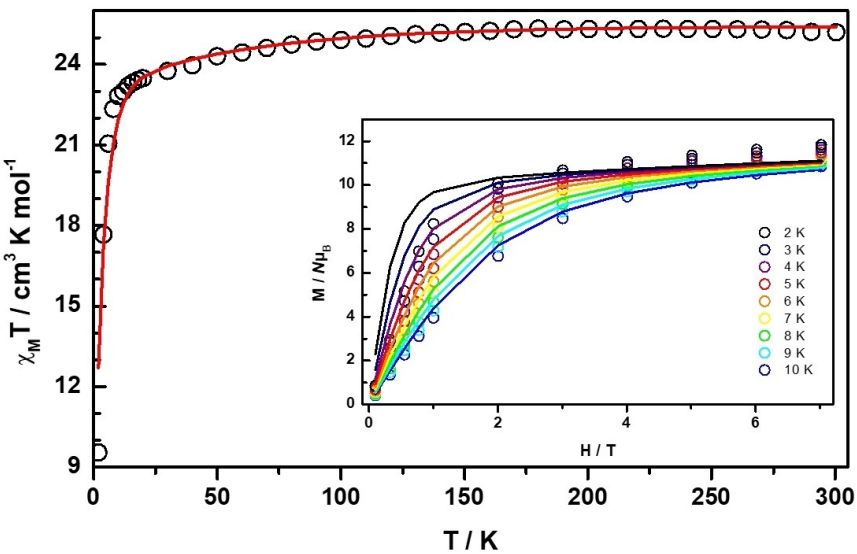

Figure 5. Temperature dependence of the $\chi_M T$ product for compound **3**. Inset: field dependence of the magnetization at various temperatures. The solid lines correspond to the best fit with the parameters indicated in the text.

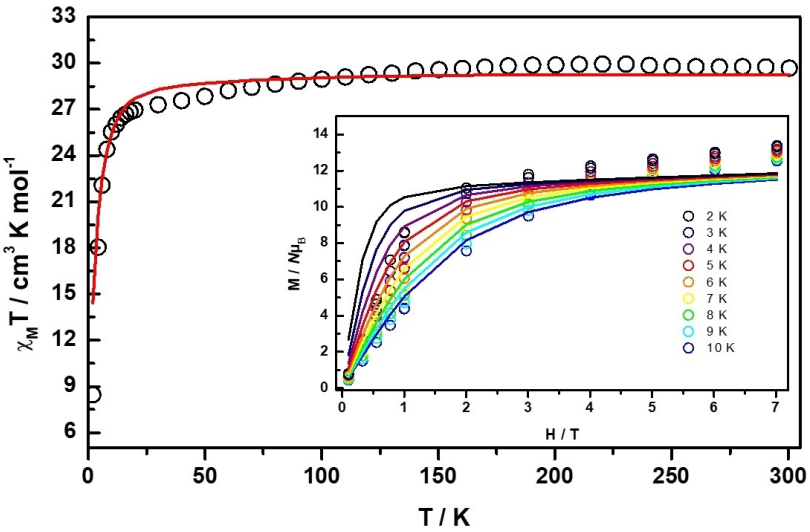

Figure 6. Temperature dependence of the $\chi_M T$ product for compound **4**. Inset: field dependence of the magnetization at various temperatures. The solid lines correspond to the best fit with the parameters indicated in the text.

geometry. However, to avoid overparameterization no further terms have been included in the fitting.

Due to the presence of magnetic anisotropy, AC measurements were performed. At zero static magnetic field only a very small out-of-phase signal was detected, which was too small to be evaluated. Therefore, field dependent AC measurements from 0 to 3000 Oe at 2 K were performed to estimate the optimum field, which was found to be 1200 Oe. Temperature dependent AC measurements were done at this static magnetic field. However, the out-of-phase signal is still very small and the AC data can be collected only up to 2.9 K (Figure 7). No maxima in the temperature dependence and Cole-Cole plots can be observed for the out-of-phase-signal. Therefore, to estimate the energy barrier, we used the Kramers-Kronig equation, that is adapted for the study of slow relaxation of the magnetization phenomena:[16]

$$\frac{\chi'}{\chi''} = \omega\tau$$

$$\frac{\chi'}{\chi''} = \omega\tau_0 + \exp\left(\frac{\Delta}{k_B T}\right)$$

$$ln\left(\frac{\chi'}{\chi''}\right) = \ln\left(\omega\tau_0\right) + \frac{\Delta}{k_B T}$$

By applying the Kramers-Kronig equation and linear fits of the natural logarithm of the ratio of the out-of-phase-signal over the in-phase-signal versus 1/T the energy barrier was estimated to be 8.2(19) cm^{-1} (Table S3).

The static magnetic properties of compound **5** (Figure 8) have been treated following the procedure applied for compounds **3** and **4**. At room temperature, a $\chi_M T$ value of 16.93 $cm^3 Kmol^{-1}$ is observed, which is higher than the expected one of 15.04 $cm^3 Kmol^{-1}$ for two non-interacting radicals $S_1 = S_2 = {}^1/_2$ and two thulium ions ($^3H_6$, $S=1$, $L=5$, $g={}^7/_6$). A very similar behaviour to the previous samples, **3** and **4**, is observed on cooling. At temperatures below 50 K the $\chi_M T$ values decrease significantly, reaching 7.93 $cm^3 Kmol^{-1}$ at 2 K. The field dependence of the magnetization shows a rapid increase at low fields without saturation at high fields, indicating strong crystal field effects. This is further confirmed by the value reached at 2 K and 7 Tesla of 8.77 $N\mu_B$, which lies below the expected value of 16 $N\mu_B$. To estimate the contribution and the sign of the CF, the magnetic data were simulated in the same manner as for **3** and **4**. First the data were simulated without any CF and then with CF (positive and negative), while fixing all the other parameters to the values obtained from compound **2**. Thereafter, all parameters (J, zJ, CF) were freely refined. In addition, fitting with varying the g values of the thulium ions were done (Figure 8). The best fit is obtained with the following parameters: $g_{Rad} = 2.000$, $g_{Tm} = 1.263(1)$, $J_{TmRad} = -0.53(1)$ cm^{-1}, $zJ = -0.0179(4)$ cm^{-1}, $B_2^0 = -4.73(19)$ cm^{-1}. The information about the Tm^{III}-Rad interaction is very scarce in literature: within one discrete binuclear complex, assembled using a nitronyl-nitroxide ligand grafted with the 5-bromo-3-pyridyl group, this interaction was estimated as being very weak ferromagnetic.[17]

The case of the europium derivative, **1**, is particularly interesting since at low temperature Eu^{III} is diamagnetic. The room temperature of the $\chi_M T$ product (3.92 $cm^3 Kmol^{-1}$) arises from the contributions of the two radicals (0.75 $cm^3 Kmol^{-1}$, $g_{Rad} = 2.000$) and of Eu^{III} ($^7F_0$, $S=3$, $L=3$), for which the first excited states are populated at room temperature and therefore it is paramagnetic. Upon cooling a nearly linear decrease of $\chi_M T$ is observed, reaching a value of 0.77 $cm^3 Kmol^{-1}$ at 2 K (Figure 9). The field dependence of the magnetization shows a rapid increase at low fields and close to saturation at high fields (inset Figure 9). The observed value at 2 K and 7 Tesla of 2.10 $N\mu_B$ is very close to the value for two non-interacting radicals $S_1 = S_2 = {}^1/_2$, while the Eu^{III} ions with $J=0$ should no contribute to the field dependence of the magnetization. At

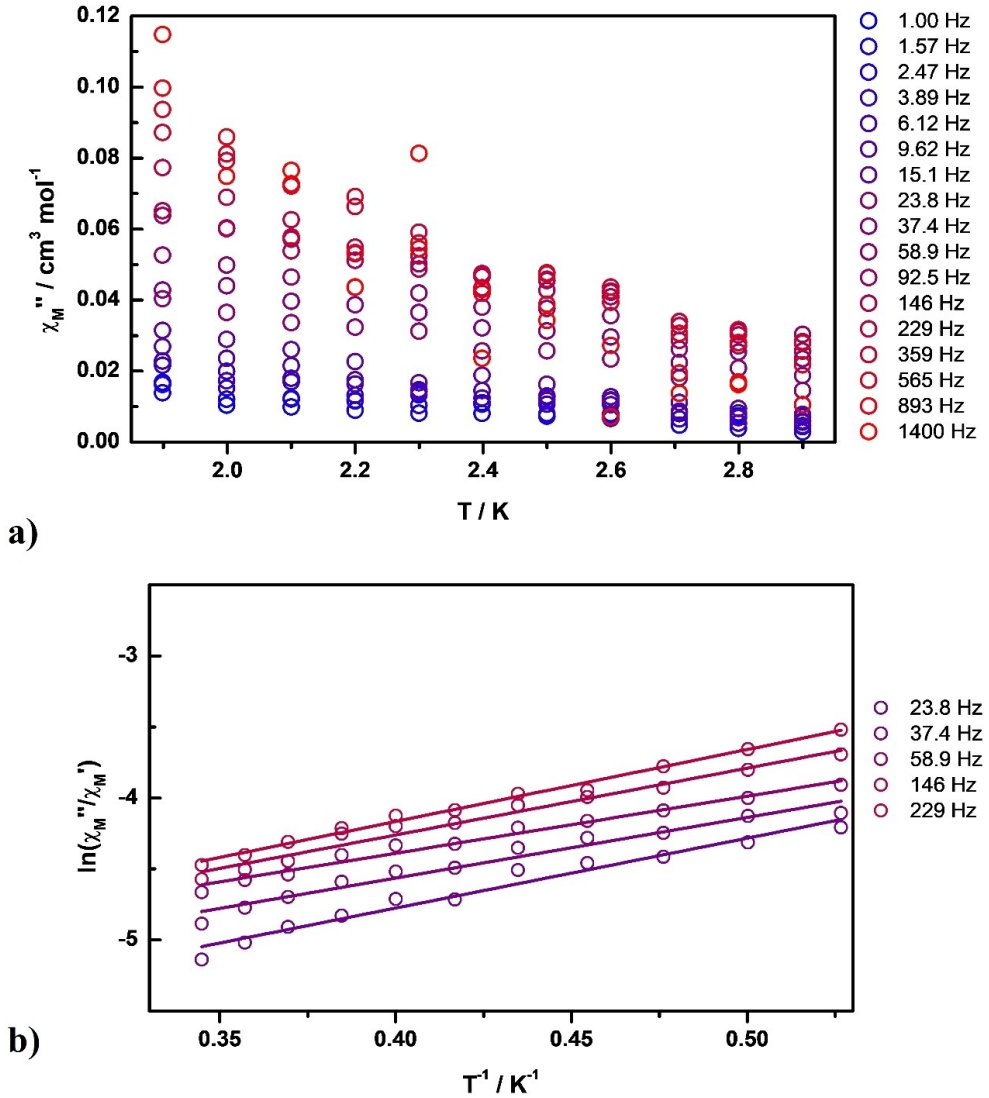

Figure 7. (a) Temperature dependence of the out-of-phase-signal at various frequencies for compound **4**; (b) Natural logarithm of the ratio of the out-of-phase-signal over the in-phase-signal versus 1/T for selected frequencies for compound **4**.

higher temperatures a certain contribution to the magnetization of the first excited states of Eu^{III} is expected.

Conclusions

The functionalization of the nitronyl-nitroxide radical with the pyrazole moiety allows the assembly of similar rectangular binuclear complexes. The metal ions are bridged by the ligand, which coordinates through one aminoxyl group to one metal ion and through the pyrazole fragment to the other one. Although the molecular structures are similar, the six compounds are grouped into two families, according to the space groups in which they crystallize: $P2_1/n$ (Gd^{III}, Eu^{III} and Tm^{III} complexes) and $P\bar{1}$ (Gd^{III}, Tb^{III}, and Dy^{III} derivatives). The crystal packing of the binuclear complexes (compounds **3** and **5**) is therefore different for the two space groups. For the Gd^{III}, Tb^{III}, and Dy^{III} derivatives the Ln^{III}-Rad exchange interaction was found ferromagnetic, while for the Tm^{III} derivative this interaction is very weak and antiferromagnetic. The potential of this ligand will be further explored towards 3*d* metal ion as well as in designing heterotrispin complexes.

Experimental Section

Materials

All reagents and solvents were reagent grade and, were used as received, without further purification.

The synthesis of 3-phenyl-1H-pyrazole-4-carbaldehyde has been performed fallowed the published procedure.[18]

Synthesis of the 5-phenylpyrazol-4-nitronyl nitroxide. To 50 ml methanolic solution containing 2 g (8.1 mmol) 2,3-bis

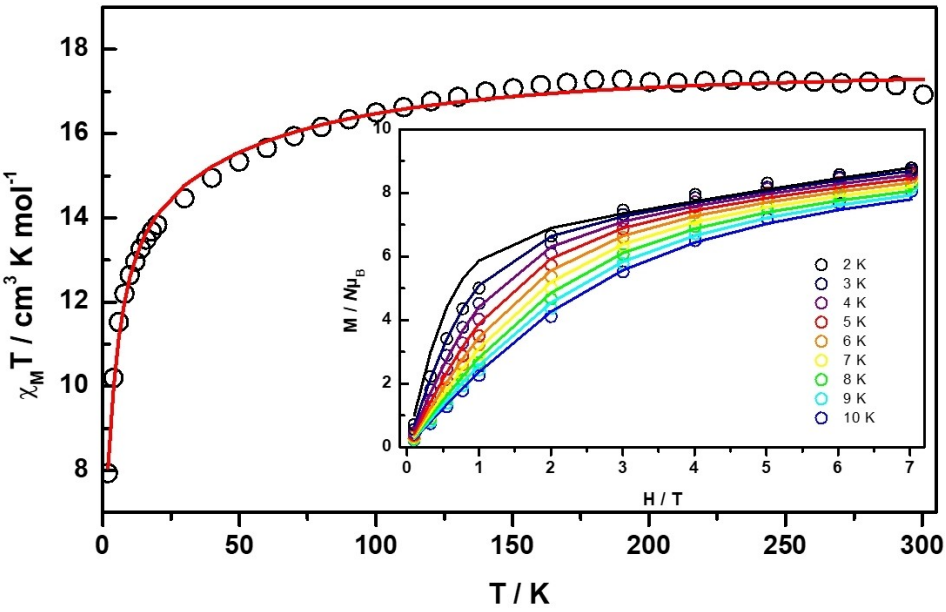

Figure 8. Temperature dependence of the $\chi_M T$ product for compound **5**. Inset: field dependence of the magnetization at various temperatures. The solid lines correspond to the best fit with the parameters indicated in the text.

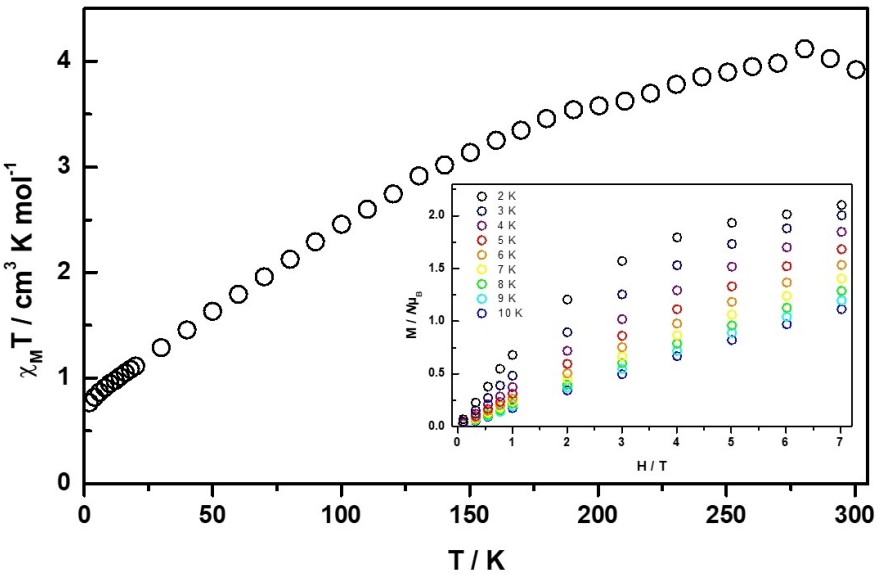

Figure 9. Temperature dependence of the $\chi_M T$ product for compound **1**. Inset: field dependence of the magnetization at various temperatures.

(hydroxyamino)-2,3-dimethylbutane sulfate deprotonated with 1 ml triethylamine, 1 g (5.8 mmol) 3-phenyl-1H-pyrazole-4-carbaldehyde was added. The resulting solution was stirred at room temperature for 48 hours and then concentrated under reduced pressure. The obtained pale-yellow oil was dissolved in 100 ml dichloromethane and under vigorous stirring at 0 °C, 0.642 g (3 mmol) sodium periodate and 2–3 ml water were added. After 15 minutes, the dark purple solution was dried over anhydrous magnesium sulfate and concentrated under reduced pressure. The dark purple-blue oil was purified by column chromatography on silica gel, using diethyl ether as eluent. The product was obtained as a dark purple sticky solid (0.50 g, 29 %).

General synthesis of 1-5 complexes. To 15 ml boiling n-heptane solution containing 0.027 g (0.033 mmol) $[M(hfac)_3(H_2O)_2]$ (M = Eu, Gd, Tb, Dy, and Tm), a dichloromethane solution (1–2 ml) of 5-phenylpyrazol-4-nitronyl nitroxide (0.01 g, 0.033 mmol) was quickly added and the mixture was stirred one minute. The resulting solution was kept at room temperature and after 3–4 days dark purple crystals were obtained. The crystals were collected by filtration, washed with n-heptane and dried in air. **1**: 3427(w), 1664 (s), 1587(m), 1535(m), 1456(m), 1271(s), 1232(s), 1159(s), 1093(w), 958(w), 810(w), 667(w), 582(w). **2**: 3374(w), 1651(m), 1611(s), 1561 (w), 1536(m), 1505(m), 1476(m), 1401(w), 1376(w), 1313(w), 1258 (vs), 1208(s), 1145(vs), 1099(w), 953(m-w), 806(m-w), 662(m-w), 586 (m-w).. **3**: 3692(m-w, br), 3375(w), 1651(s), 1603(w), 1561(m), 1534

(m), 1505(m), 1477(m), 1401(w), 1375(w), 1313(w), 1258(vs), 1207(s), 1146(vs), 1100(w), 953(m-w), 805(m-w), 663(m-w), 587(m-w) **4** IR data (KBr pellet, cm^{-1}): 3690(m–w, br), 3377(w), 2965(m-w), 1651(s), 1603(w), 1560(m), 1534(m), 1506(m), 1477(m), 1401(w), 1375(w), 1314(w), 1258(vs), 1207(s), 1146(vs), 1100(w), 953(m-w), 804(m-w), 662(m-w), 587(m-w). **5**: 3390(w), 1652(s), 1562(s), 1537(m), 1479(m), 1261(s), 1215(s), 1149(s), 1107(w), 956(w), 804(w), 661(w), 586(w). In the case of the gadolinium - radical system, two types of crystals were observed (**2a** and **2b**), but only for **2a** we succeeded to have a good crystal structure. For the polymorph **2b** only the unit cell parameters were measured.

Physical measurements

IR spectra were performed on a FTIR Bruker Tensor V-37 spectrophotometer (KBr pellets) in the range of 4000–400 cm^{-1}. X-ray powder diffraction data were recorded on PANalytical Empyrean diffractometer at 298 K. DC and AC magnetic studies for all compounds were performed with a Quantum Design MPMS-XL-7 SQUID magnetometer on powdered microcrystalline samples. The sample **4** was embedded in eicosane to avoid orientation of the crystallites under applied field. Experimental susceptibility data were corrected for the underlying diamagnetism using Pascal's constants. The temperature dependent magnetic contribution of the holder and in case of **4** of the embedding matrix eicosane were experimentally determined and subtracted from the measured susceptibility data. Variable temperature susceptibility data were collected in a temperature range of 2–300 K under an applied field of 0.1 Tesla, while magnetization data were collected between 2 and 10 K and magnetic fields up to 7 Tesla. AC measurements were performed with an oscillating magnetic field of 3 Oe at frequencies ranging from 1 to 1400 Hz. Field dependent AC susceptibility for **3**, **4**, **5** and **1** were measured at 2 K and magnetic fields from 0 to 3000 Oe to determine the optimum field. The optimum static magnetic field for **4** is 1200 Oe, while at zero Oe a neglectable AC signal was detected. No Ac signal was detected for **4** and **5** neither at zero nor at applied field up to 3000 Oe. The magnetic data were fitted with the help of the program PHI.[19] while the AC data were fitted with the Kramers-Kronig equation.

X-Ray data collection and crystal structure refinement

Crystallographic data were collected on a STOE IPDS II diffractometer (**3** and **5**) and a Bruker APEX-II CCD (**2a** and **4**) using graphite-monochromated Mo–Kα radiation ($\lambda = 0.71073$ Å). The structures were solved by direct methods and refined by full-matrix least squares techniques based on F^2. The non-H atoms were refined with anisotropic displacement parameters. The H atoms attached to carbon were set in calculated positions and refined using the riding model. Calculations were performed using SHELXT and SHELXL-2015 crystallographic software packages.[20]

Deposition Numbers 2044705 (for **2a**), 2044706 (for **3**), 2044707 (for **4**), and 2010169 (for (**5**) contain the supplementary crystallographic data for this paper. These data are provided free of charge by the joint Cambridge Crystallographic Data Centre and Fachinformationszentrum Karlsruhe Access Structures service www.ccdc.cam.ac.uk/structures.

Acknowledgements

*S.C. is grateful to the University of Bucharest (ICUB) for a postdoctoral fellowship. J.C. da R. thank Fundação de Amparo à Pesquisa do Estado do Rio de Janeiro (FAPERJ) for a postdoctoral fellowship. Financial support from the following grants is gratefully acknowledged: Project PN-III-P4-ID-PCE-2016-0308 (UEFISCDI – Romania), Coordenação de Aperfeiçoamento de Pessoal de Nível Superior – Brazil (CAPES) within the scope of the Capes-PrInt Program – Universidade Federal Fluminense – Financial Code 001, project number: 88887.310269/2018-00. We are also thankful for the financial support of the Brazilian agencies Conselho Nacional de Desenvolvimento Científico e Tecnológico (CNPq) and FAPERJ. Authors also would like to thank MSc Francielli Sousa Santana (Laboratório de Difratometria de Raios X de Monocristal, Universidade Federal do Paraná) for the crystallographic data collection for compounds **2** and **4**. Open access funding enabled and organized by Projekt DEAL.*

Conflict of Interest

The authors declare no conflict of interest.

Keywords: Nitronyl-nitroxide ligands · Lanthanides complexes · Magnetic properties · Metallarectangles

[1] a) D. Luneau, *Eur. J. Inorg. Chem.* **2020**, 597; b) S. Demir, I.-R. Jeon, J. R. Long, T. D. Harris, *Coord. Chem. Rev.* **2015**, *289–290*, 149; c) X. Meng, W. Shi, P. Cheng, *Coord. Chem. Rev.* **2019**, *378*, 134; d) M. T. Lemaire, *Pure Appl. Chem.* **2004**, *76*, 277; e) C. Benelli, D. Gatteschi, *Chem. Rev.* **2002**, *102*, 2369; f) D. Luneau, P. Rey, *Coord. Chem. Rev.* **2005**, *249*, 2591; g) A. Caneschi, D. Gatteschi, R. Sessoli, P. Rey, *Acc. Chem. Res.* **1989**, *22*, 392.

[2] A. Caneschi, D. Gatteschi, N. Lalioti, C. Sangregorio, R. Sessoli, G. Venturi, A. Vindigni, A. Rettori, M. G. Pini, M. A. Novak, *Angew. Chem. Int. Ed.* **2001**, *40*, 1760.

[3] a) J. H. Osiecki, E. F. Ullman, *J. Am. Chem. Soc.* **1968**, *90*, 1078; b) E. F. Ullman, L. Call, J. H. Osiecki, *J. Org. Chem.* **1970**, *35*, 3623; c) E. F. Ullman, J. H. Osiecki, D. G. B. Boocock, R. Darcy, *J. Am. Chem. Soc.* **1972**, *94*, 7049; d) C. Hirel, K. E. Vostrikova, J. Pécaut, V. I. Ovcharenko, P. Rey, *Chem. Eur. J.* **2001**, *7*, 2007.

[4] See, for example: a) M. G. F. Vaz, A. Akpinar, G. P. Guedes, S. Santos Jr., M. A. Novak, P. M. Lahti, *New J. Chem.* **2013**, *37*, 1927; b) L. Tian, Y.-Q. Sun, B. Na, P. Cheng, *Eur. J. Inorg. Chem.* **2013**, 4329; c) K. Bernot, F. Pointillart, P. Rosa, R. Sessoli, D. Gatteschi, *Chem. Commun.* **2010**, *46*, 6458; d) Z.-X. Xiao, H. Miao, D. Shao, H.-Y. Wei, Y.-Q. Zhang, X.-Y. Wang, *Chem. Commun.* **2018**, *54*, 9726; e) A. Caneschi, D. Gatteschi, J. Laugier, L. Pardi, P. Rey, C. Zanchini, *Inorg. Chem.* **1988**, *27*, 2027; f) D. Luneau, F. M. Romero, R. Ziessel, *Inorg. Chem.* **1998**, *37*, 5078.

[5] See, for example: a) J. Sun, Z. Sun, L. Li, J.-P. Sutter, *Inorg. Chem.* **2018**, *57*, 7507; b) G. P. Guedes, R. G. Zorzanelli, N. M. Comerlato, N. L. Speziali, S. Santos-Jr., M. G. F. Vaz, *Inorg. Chem. Commun.* **2012**, *23*, 59; c) H. Miao, M. Li, H.-Q. Li, F.-X. Shen, Y.-Q. Zhang, X.-Y. Wang, *Dalton Trans.* **2019**, *48*, 4774; d) Y.-F. Wang, L.-Y. Wang, L.-F. Ma, *Z. Anorg. Allg. Chem.*, **2008**, *634*, 181; e) P. Y. Chen, M. Z. Wu, T. Li, X. J. Shi, L. Tian, Z. Y. Liu, *Inorg. Chem.* **2018**, *57*, 12466; f) P. Hu, X. Wang, Y. Ma, Q. Wang, L. Li, D. Liao, *Dalton Trans.* **2014**, *43*, 2234; g) J. Omata, T. Ishida, D. Hashizume, F. Iwasaki, T. Nogami, *Inorg. Chem.* **2000**, *40*, 3954; h) Z. Liu, Z. Lu, D. Zhang, Z. Jiang, L. Li, C. Liu, D. Zhu, *Inorg. Chem.* **2004**, *43*, 6620; i) F. Furui, S. Suzuki, M. Kozaki, D. Shiomi, K. Sato, T. Takui, K. Okada, E. V. Tretyakov, S. E. Tolstikov, G. V. Romanenko, V. I. Ovcharenko, *Inorg. Chem.* **2014**, *53*, 802; j) A. Lannes, M. Intissar, Y. Suffren, C. Reber, D. Luneau, *Inorg. Chem.* **2014**, *53*, 9548; k) J. Guo, J. Sun, G. Sun, Z. Sun, L. Li, *Eur. J. Inorg. Chem.* **2018**, 3241; l) V. Ovcharenko, O. Kuznetsova, E. Fursova, G. Letyagin, G. Romanenko, A. Bogomyakov, E. Zueva, *Inorg. Chem.* **2017**, *56*, 14567.

[6] See, for example: a) L. B. L. Escobar, G. P. Guedes, S. Soriano, N. L. Speziali, A. K. Jordão, A. C. Cunha, V. F. Ferreira, C. Maxim, M. A. Novak, M. Andruh, M. G. F. Vaz, *Inorg. Chem.* **2014**, *53*, 7508; b) M. Zhu, L. Li, J.-P. Sutter, *Inorg. Chem. Front.* **2016**, *3*, 994; c) L. Xi, J. Suan, K. Wang, J. Lu, P. Jing, L. Li, *Dalton Trans.* **2020**, *49*, 1089; d) G. Novitchi, S. Shova, Y.

Lan, W. Wernsdorfer, C. Train, *Inorg. Chem.* **2016**, *55*, 12122; e) M. G. F. Vaz, M. Andruh, *Coord. Chem. Rev.* **2021**, *427*, 213611.
[7] a) A. A. Patrascu, S. Calancea, M. Briganti, S. Soriano, A. M. Madalan, R. A. A. Cassaro, A. Caneschi, F. Totti, M. G. F. Vaz, M. Andruh, *Chem. Commun.* **2017**, *53*, 6504; b) A. A. Patrascu, M. Briganti, S. Soriani, S. Calancea, R. A. A. Cassaro, F. Totti, M. G. F. Vaz, M. Andruh, *Inorg. Chem.* **2019**, *58*, 13090.
[8] a) R. Li, C. Zhang, D. Liao, J.-P. Sutter, *Dalton Trans.* **2012**, *41*, 12139; b) R. Liu, L. Liu, D. Fang, J. Xu, S. Zhao, W. Xu, *Anorg. Allg. Chem.* **2015**, *641*, 728; c) X. Mei, X. Wang, J. Wang, Y. Ma, L. Li, D. Liao, *New J. Chem.* **2013**, *37*, 3620.
[9] a) P. Y. Chen, X. J. Shi, T. Li, L. Tian, Z. Y. Liu, F. Z. Hua, S. J. Iu, Y. Y. Su, *RSC Adv.* **2017**, ***7***, 45504; b) P. Y. Chen, X. J. Shi, T. Li, L. Tian, *Inorg. Chem. Commun.* **2017**, *86*, 58; c) F. Pointillart, K. Bernot, G. Poneti, R. Sessoli, *Inorg. Chem.* **2012**, *51*, 12218; d) J. Song, P. Hu, L.-J. Zhang, Z.-Y. Liu, J. Yu, R.-J. Xie, L.-Z. Huang, Y.-Y. Gao, *Inorg. Chem. Commun.* **2019**, *105*, 188; e) M. Zhu, Y. Li, L. Jia, L. Zhang, W. Zhanh, *RSC Adv.* **2017**, ***7***, 36895.
[10] a) J. Wang, H. Miao, Z.-X. Xiao, Y. Zhou, L.-D. Deng, Y.-Q. Zhang, X.-Y. Wang, *Dalton Trans.* **2017**, *46*, 10452; b) H. Miao, H.-Q. Li, F.-X. Shen, H.-Y. Wei, B.-L. Wang, X.-Y. Wang, *Dalton Trans.* **2019**, *48*, 10337.
[11] J. Pérez, L. Riera, *Eur. J. Inorg. Chem.* **2009**, 4913.
[12] a) D. Casanova, J. Cirera, M. Llunell, P. Alemany, D. Avnir, S. Alvarez, *J. Am. Chem. Soc.* **2004**, *126*, 1755; b) D. Casanova, M. Llunell, P. Alemany, S. Alvarez, *Chem. Eur. J.* **2005**, *11*, 1479; c) M. Llunell, D. Casanova, J. Circra, J. M. Bofill, P. Alcmany, S. Alvarez, M. Pinsky, D. Avnir, *SHAPE*, version 2.1, University of Barcelona, Barcelona, Spain, and Hebrew University of Jerusalem, Jerusalem, Israel, **2005**.
[13] A. Bondi, *J. Phys. Chem.*, **1964**, *68*, 441.
[14] A. Abragam, B. Bleaney, *Electron Paramagnetic Resonance*, Clarendon Press, Oxford, UK, **1970**.
[15] T. Gupta, T. Rajashkumar, G. Rajaraman, *Phys. Chem. Chem. Phys.* **2014**, *16*, 14568.
[16] J. Bartolomé, G. Filoti, V. Kuncser, G. Schinteie, V. Mereacre, C. E. Anson, A. K. Powell, D. Prodius, C. Turta, *Phys. Rev. B* **2009**, 80.014430.
[17] J.-X. Xu, Y. Ma, D.-z. Liao, G.-F. Xu, J. Tang, C. Wang, N. Zhou, S.-P. Yan, P. Cheng, L.-C. Li, *Inorg. Chem.* **2009**, *48*, 8890.
[18] A. V. Lebedev, A. B. Lebedeva, V. D. Sheludyakov, E. A. Kovaleva, O. L. Ustinova, I. B. Kozhevnikov, *Russ. J. Gen. Chem.* **2005**, *75*, 782.
[19] N. F. Chilton, R. P. Anderson, L. D. Turner, A. Soncini, K. S. Murray, *J. Comput. Chem.* **2013**, *34*, 1164.
[20] a) G. M. Sheldrick, *Acta Crystallogr.* **2015**, *A71*, 3; b) G. M. Sheldrick, *Acta Crystallogr.* **2015**, *C71*, 3.

Manuscript received: October 13, 2020
Revised manuscript received: November 26, 2020
Accepted manuscript online: November 26, 2020